

J-PLUS: Support Vector Machine Applied to STAR-GALAXY-QSO Classification

Cunshi Wang^{1,2}, Yu Bai¹, C. López-Sanjuan⁸, Haibo Yuan³, Song Wang¹, Jifeng Liu^{1,2}, David Sobral⁴, P. O. Baqui⁵, E. L. Martín^{15,6,7}, Carlos Andres Galarza¹⁰, J. Alcaniz¹⁰, R. E. Angulo^{11,12}, A. J. Cenarro⁸, D. Cristóbal-Hornillos⁸, R. A. Dupke^{10,13,14}, A. Ederoclite⁹, C. Hernández-Monteagudo^{15,6}, A. Marín-Franch⁸, M. Moles⁸, L. Sodré Jr.⁹, H. Vázquez Ramíó⁸, and J. Varela⁸

¹ Key Laboratory of Optical Astronomy, National Astronomical Observatories, Chinese Academy of Sciences, 20A Datun Road, Chaoyang District, Beijing 100012, People's Republic of China

² College of Astronomy and Space Sciences, University of Chinese Academy of Sciences, Beijing 100049, China

³ Department of Astronomy, Beijing Normal University, Beijing 100875, People's Republic of China

⁴ Department of Physics, Lancaster University, Lancaster LA1 4YB, UK

⁵ PPGFis & Núcleo de Astrofísica e Cosmologia (Cosmo-ufes), Universidade Federal do Espírito Santo, 29075-910 Vitória, ES, Brazil

⁶ Departamento de Astrofísica, Universidad de La Laguna (ULL), E-38206 La Laguna, Tenerife, Spain

⁷ Consejo Superior de Investigaciones Científicas (CSIC), E-28006 Madrid, Spain

⁸ Consejo Superior de Investigaciones Científicas (CSIC), E-28006 Madrid, Spain Centro de Estudios de Física del Cosmos de Aragón (CEFCA), Unidad Asociada al CSIC, Plaza San Juan 1, 44001 Teruel, Spain

⁹ Instituto de Astronomia, Geofísica e Ciências Atmosféricas, Universidade de São Paulo, 05508-090 São Paulo, Brazil

¹⁰ Observatório Nacional - MCTI (ON), Rua Gal. José Cristino 77, São Cristóvão, 20921-400 Rio de Janeiro, Brazil

¹¹ Donostia International Physics Centre (DIPC), Paseo Manuel de Lardizabal 4, 20018 Donostia-San Sebastián, Spain

¹² IKERBASQUE, Basque Foundation for Science, 48013, Bilbao, Spain

¹³ University of Michigan, Department of Astronomy, 1085 South University Ave., Ann Arbor, MI 48109, USA

¹⁴ University of Alabama, Department of Physics and Astronomy, Gallalee Hall, Tuscaloosa, AL 35401, USA

¹⁵ Instituto de Astrofísica de Canarias, La Laguna, 38205, Tenerife, Spain

July 10, 2022

ABSTRACT

Context. In modern astronomy, machine learning has proved to be efficient and effective to mine the big data from the newest telescopes. Spectral surveys enable us to characterize millions of objects, while long exposure time observations and wide surveys constrain their strides from millions to billions.

Aims. In this study, we construct a supervised machine learning algorithm, to classify the objects in the Javalambre Photometric Local Universe Survey first data release (J-PLUS DR1).

Methods. The sample set is featured with 12-waveband photometry, and magnitudes are labeled with spectrum-based catalogs, including Sloan Digital Sky Survey spectroscopic data, Large Sky Area Multi-Object Fiber Spectroscopic Telescope, and VERONCAT - Veron Catalog of Quasars & AGN. The performance of the classifier is presented with applications of blind test validations based on Radial Velocity Extension, Kepler Input Catalog, 2 MASS Redshift Survey, and the UV-bright Quasar Survey. A new algorithm is applied to constrain the extrapolation that could decrease accuracies for many machine learning classifiers.

Results. The accuracies of the classifier are 96.5% in blind test and 97.0% in training cross validation. The F_1 -scores for each class are presented to show the precision of the classifier. We also discuss different methods to constrain the potential extrapolation.

Key words. methods: data analysis – techniques: spectroscopic - astronomical databases: miscellaneous

1. Introduction

The computer science and the technological applications have changed the ways of data processing and knowledge management. Especially, as a raising realm of technology, machine learning has gained worldwide popularity due to its powerful ability to manage large amounts of data. Machine learning algorithms can reveal potential patterns and physical meanings that are otherwise indistinguishable by traditional methods. Furthermore, machine learning enables us to construct structure of each observed quantity and to reveal its manner of working.

In modern astronomy, the newest telescopes have produced large amounts of unprocessed data. The Javalambre Photomet-

ric Local Universe Survey (J-PLUS, Cenarro et al. 2019) is designed to observe several thousand square degrees in the optical. It has been used to designed to observe more than 13 million objects with JAST/T80 at the Sierra de Javalambre in Spain. It has been used to achieve knowledge from the solar system to cosmology¹, such as the coma cluster (Jiménez-Teja et al. 2019), low-metallicity stars (Whitten et al. 2019), and galaxy formation (Nogueira-Cavalcante et al. 2019).

The current classification of sources detected by J-PLUS is morphological, this is, aims to distinguish between point-like and extended sources (Cenarro et al. 2019; López-Sanjuan

¹ <http://j-plus.es/survey/science>

et al. 2019). It is not able therefore to differentiate stars from quasars (QSO), and does not include the valuable colour information from the 12 optical J-PLUS bands. This paper presents the spectrum-based classification for J-PLUS first data release (DR1) with machine learning algorithms. The input catalog is from a modified version of J-PLUS data set that has been recalibrated by Yuan (2021). This version includes 13,265,168 objects with magnitudes obtained with 12 different filters (Section 2.1). From Section 2.2 to 2.4, we label the data set as STAR, GALAXY, and QSO based on spectroscopy surveys, including Sloan Digital Sky Survey (SDSS), Large Sky Area Multi-Object Fiber Spectroscopy Telescope (LAMOST), and VERONCAT - Veron Catalog of Quasars & AGN.

Several machine learning algorithms have been applied for the classification (Section 3), including Support Vector Machine (SVM, Cortes & Vapnik 1995), linear discrimination, k-nearest neighbor (k-NN, Cover & Hart 1967; Stone 1977), Bayesian, and decision trees (Quinlan 1986). We present the processes to test the parameters of the algorithms and to train the classifier (Section 3.1). We also provide the blind test and a method to constrain extrapolation (Section 3.2) in prediction. The extrapolation is constrained in the final decision.

We present our result in Section 4. In Section 5, we discuss different methods to constrain the extrapolation. The classifier is compared with other published classifiers, and the difference is analyzed in detail (Section 5.2). Section 5.3 gives an outlook of Javalambre Physics of the Accelerating Universe Astrophysical Survey (J-PAS, Benítez et al. 2014; Bonoli et al. 2021) and our future work.

2. Data

The rapid advance in telescopes and detectors has led to a significant data explosion in modern astronomy. New technologies help us accelerate information acquisition and enlarge the data set volume. Several studies have focused on developing classifiers, and it has been shown that spectrally based methods are more reliable than those only based on photometric data (Bai et al. 2018; Ball et al. 2006).

2.1. J-PLUS

J-PLUS² is being conducted from the Observatorio Astrofísico de Javalambre (OAJ, Teruel, Spain; Cenarro et al. 2014) using the 83 cm Javalambre Auxiliary Survey Telescope (JAST80) and T80Cam, a panoramic camera of $9.2\text{k} \times 9.2\text{k}$ pixels that provides a 2deg^2 field of view (FoV) with a pixel scale of $0.55\text{ arcsec pix}^{-1}$ (Marín-Franch et al. 2015). The J-PLUS filter system is composed of twelve passbands, including five broad and seven medium bands from 3000 to 9000 Å. The J-PLUS observational strategy, image reduction, and main scientific goals are presented in Cenarro et al. (2019). J-PLUS DR1 covers a sky area of $1,022\text{ deg}^2$, and the limiting magnitudes are in the range 21–22. For different kinds of objects, the magnitudes of these 12 bands exhibit different distributions³, and such difference gives us a theoretical foundation of object classification.

The J-PLUS catalog is an ideal data set for classification owing to its large amount and more wavebands than any existing photometric survey. More bands could provide more information for a single object. In machine learning, these 12-band magnitudes lead to a more expanding training instance space and a

smoother training structure. We adopt the 12 band magnitudes as training features, which are u , $J0378$, $J0395$, $J0410$, $J0430$, g , $J0515$, r , $J0660$, i , $J0861$, z . We name them as mag1 through to mag12 .

Recently, Yuan (2021) has recalibrated the J-PLUS catalog and increased the accuracy of photometric calibration by using the method of Stellar Color Regression, similar to the method in Yuan et al. (2015). The catalog in Yuan (2021) contains 13,265,168 objects, including 4,126,928 objects with full 12 magnitudes.

2.2. SDSS

SDSS has covered one-third of the sky, and yielded more than 3 million spectra. We explore the spectroscopy survey sets in data release 16 (DR16; Ahumada et al. 2020). With the help of SDSS Catalog Archive Server Jobs⁴, the objects with $z_{\text{Warning}} = 0$ are chosen to label the J-PLUS data as “STAR”, “GALAXY”, and “QSO”.

The Apache Point Observatory Galactic Evolution Experiment (APOGEE) has observed more than a hundred thousand stars in Milky Way, with reliable spectral information including stellar parameters and radial velocities (Zasowski et al. 2013). We adopt the APOGEE catalog to enlarge the training set.

We cross match J-PLUS catalog with SDSS DR16 using Tool for Operations on Catalogues And Tables (Topcat)⁵ with a tolerance of 1 arcsec, and obtain 63,399 stars, 171,785 galaxies and 69,851 QSOs from the general catalog, and 13,838 stars from APOGEE. Totally, SDSS contributes with 318,873 objects.

2.3. LAMOST

LAMOST (Cui et al. 2012; Luo et al. 2012; Zhao et al. 2012; Guan Wang et al. 1996; Su & Cui 2004) is settled at Xinglong Observatory, China, which is able to observe 4,000 objects in 20deg^2 simultaneously. LAMOST has many scientific projects, and two of them aim at understanding the structure of Milky Way (Deng et al. 2012) and external galaxies. The low resolution spectra of LAMOST have a limiting magnitude of about 20 in g band for resolution $R=500$. The Data Release 7 (DR7) is adopted to label the sample. We also expand the sample with stellar catalogs from DR7, including A-, F-, G- and K- type stars catalog, A- and M- star catalogs.

The A-, F-, G- and K- type star catalog has stars with g band signal to noise ratio higher than 6 in dark nights or 15 in bright nights. The A-, and M- star catalogs contain all A and M stars from the pilot and general surveys. For overlapping stars, we follow the priority of the star catalogs, and the general catalog.

In LAMOST DR7 catalog, the cross match yields 307,189 stars, 16,396 galaxies and 4,922 QSOs. There are 212,754 matched stars in A-, F-, G- and K- type stars catalog, 5,160 and 30,227 stars in the A- and M- star catalogs, respectively.

2.4. QSO catalog

VV13 (VERONCAT - Veron Catalog of Quasars & AGN, the 13th edition) is also employed to enlarge our QSO data. It contains AGN objects with spectroscopic parameters (Véron-Cetty & Véron 2010), including red shift, and AGN types. The VV13 contains 5,174 QSOs after a 1 arcsec tolerance cross identification with J-PLUS.

² www.j-plus.es

³ http://j-plus.es/datareleases/data_release_dr1

⁴ <http://skyserver.sdss.org/casjobs/>

⁵ <http://www.star.bris.ac.uk/~mbt/topcat/>

Table 1. Constitution of Sample

Catalog	STAR	GALAXY	QSO	Total
SDSS DR16	63,399	171,785	69,851	305,035
SDSS APOGEE	13,838	0	0	13,838
LAMOST DR7	307,189	16,396	4,922	328,507
LAMOST A-, F-, G- and K- type stars	212,754	0	0	212,754
LAMOST A- stars	5,160	0	0	5,160
LAMOST M- stars	30,227	0	0	30,227
VV13	0	0	5,174	5,174

Notes. The numbers reveal how many objects are there corresponding to each catalog and class, after crossing with J-PLUS catalog. The sample contains 468,685 objects with full 12 magnitudes from the catalogs, with 348,085 STAR, 74,701 GALAXY and 45,899 QSO. There are repeated objects in different catalogs, which cause the inequality the sum. This table presents all objects for training and testing, which is a 10-fold validation. See 3.2.2 for blind test.

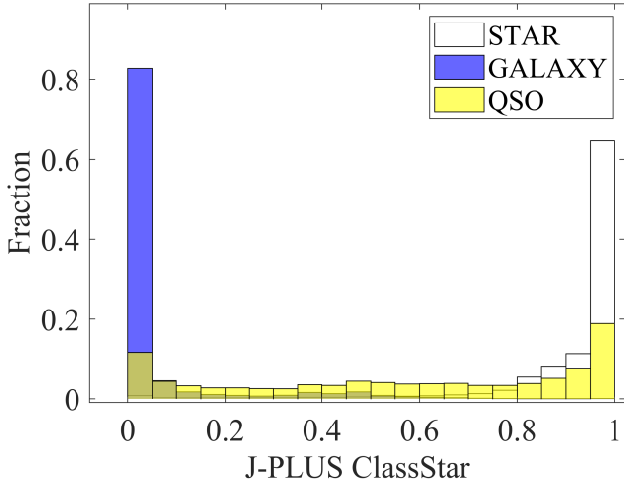


Fig. 1. The comparison between the class in the sample and J-PLUS "Class_Star" parameter. The white denotes the stellar objects, and the blue stands for the galaxies in our training sample. The yellow is the QSOs. The distributions are normalized for clarity.

The machine learning sample is constructed with SDSS, LAMOST and VV13 (Table 1, See more in Appendix C). There are 468,685 unique objects with valid 12 magnitudes, including 74,701 galaxies, 45,899 QSOs and 348,085 stars. These 468,685 objects are all put in training with a 10-fold testing. The blind test set is constructed by other catalogs for validation with 4,691 objects, see 3.2.2. J-PLUS DR1 contains the stellar probability CLASS_STAR, estimated by SExtractor (Bertin & Arnouts 1996) with an artificial neural network (ANN). We present the comparison between the probability and the classification of the sample in Fig. 1. About 20% QSO have a stellar probability more than 90%, and more than 10% QSO have a stellar probability less than 10%. The difference may ascribe to the classification strategy of J-PLUS, which is based on morphological classifier, and such strategy is probably ineffective to distinguish QSOs from stars or galaxies.

3. Methodology

Machine learning has developed many algorithms that are able to deal with the big data effectively. Three of them, decision trees, SVM, and k-NN are the most popular ones.

Table 2. Accuracy and Time cost for each algorithms

Algorithm	Accuracy	Time Cost
Decision Tree	92.6%	96s
Linear Discrimination	86.9%	26s
Bayesian	74.3%	10s
SVM	96.4%	90m
k-NN	95.7%	23m
AdaBoost	92.0%	3m
Random Forest	96.2%	7m

Notes. The last column is the rough training time cost for the training sample. The 's' stands for second, 'm' for minute. See FISHER (1936) for detail of linear discrimination algorithm, and Freund & Schapire (1995) for AdaBoost. The decision tree is based on Gini index (Quinlan 1986), and its maximum split is equal to 100. The AdaBoost algorithm contains 30 learners with learning rate 0.1, and has a maximum split of 20. The Random Forest (RF, Breiman 2001) algorithm also contains 30 learners and maximum splits to 468684. Hyperparameters are not involved in all tree algorithms. In k-NN, we employ a 10-NN algorithm with Euclid norm, no hyperparameters or weights involved. The SVM algorithm is based on a gaussian kernel with kernel scale 0.87. All the algorithms are trained without weights or hyperparameters.

3.1. SVM

SVM is a binary classification method, see Cortes & Vapnik (1995) and Boser et al. (1992) for detail. The theory of SVM is presented in Cristianini & Shawe-Taylor (2000) and Shalev-Shwartz & Ben-David (2014).

In brief, SVM algorithm generates a super surface in the instance space by maximizing the margin. The margin is defined by the smallest distance between the object and the super surface. Given a super surface, the algorithm divides the instance space into two parts, and labels the object in each part. The algorithm then compares each label with the sample and calculates the loss function. The margin is maximized when the loss function reaches its minimum. For our classification problem, there are 12 dimensions in the instance space.

SVM is a binary classification algorithm, while our problem is multi-classification. Coding method can change a multi-classification problem into several binary classifications, such as one-vs-one coding and one-vs-all coding. For a k-classification problem, the one-vs-one coding finds all binary combinations of the labels. After making a democratic decision, the algorithm produces the predicted label. The one-vs-one coding needs $\frac{k(k-1)}{2}$ binary classifications to reach the aim. One-vs-all coding singly

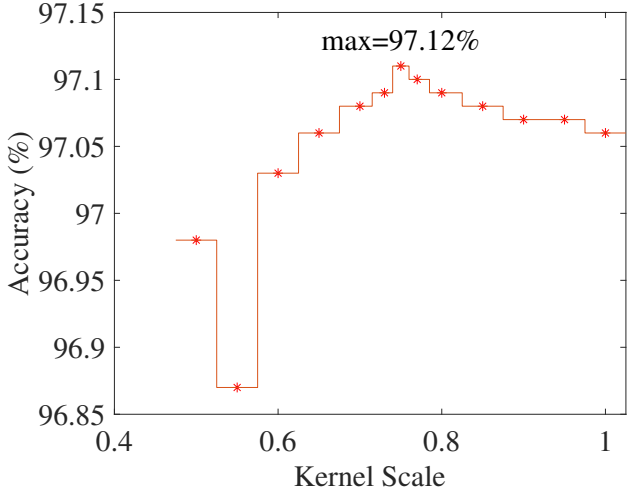


Fig. 2. Different kernel scales and its corresponding accuracies. The maximum is at 0.75.

True Label	GALAXY	70747	1138	2816	94.7%	5.3%
	QSO	1064	42370	2465	92.3%	7.7%
	STAR	2199	4345	341541	98.1%	1.9%
		GALAXY	QSO	STAR		
		Predict Label				

Fig. 3. The training confusion matrix. The blue rectangles show the correct labels, while the pinks represent the error labels.

picks one label out and defines it as positive class, and the rest $(k - 1)$ labels are negative. After k times binary classifications, the one-vs-all coding presents the labels by democratic decision. The one-vs-one coding has a higher accuracy in our classification.

Gaussian kernel, also known as radial basis function (RBF) kernel, is an important parameter in the SVM algorithm construction. It can accelerate the optimization of margin in SVM algorithm. In gaussian kernel, a kernel scale is an adjustable factor that measures the distance to the half-space. A small kernel scale constrains the kernel function in low variation, and further parameterizes the margin exquisitely. The farther the data points locate from the margin, the less weight they have. In order to find the best kernel scale, we test the scale from 0.5 to 1, with a step size of 0.05. For each kernel scale, we train a classifier and calculate an accuracy. Finally, we conclude that 0.75 is the best kernel scale (Fig. 2).

The magnitude uncertainties in J-PLUS DR1 (Yuan 2021) depend on the observing condition and the photometric calibration. In our training process, we employ the uncertainties as the training weight to describe the reliability of the data.

In order to find the best classifier, several classification algorithms are tested with 10-fold-validation. We examine the accu-

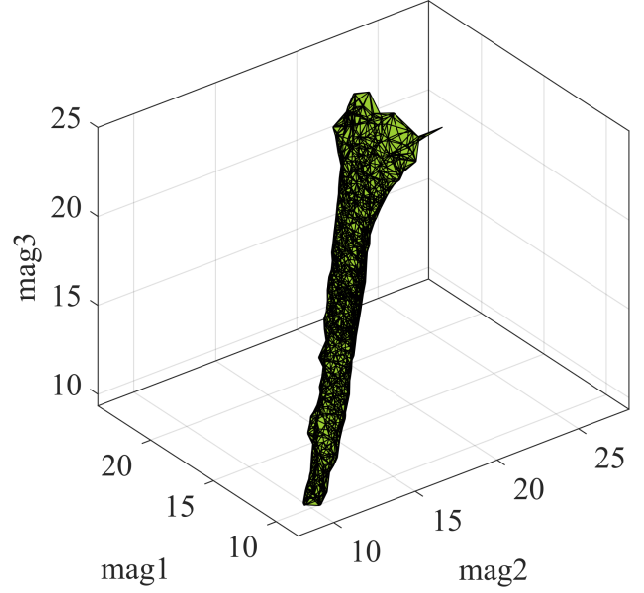


Fig. 4. The density contour of the first 3 magnitudes of the training data set. The contour stands for the three-dimensional density of 5% of the training data.

racy and training time cost of each method (Table 2), and then adopt SVM algorithm that has the highest accuracy of validation.

The confusion matrix is shown in Fig. 3. The total cross validation accuracy is 97%. The low accuracy of QSO may be due to its relatively small sample size.

3.2. Validation

Model validation has been designed to show the effectiveness and to avoid potential overfitting. Extrapolation is significant in model validation. It has been proved that the prediction accuracy might decrease, when extrapolating outside the feature space region of training samples (Wang 2021). The other validating procedure is blind test, which can reveal the potential overfitting of the classifier. Moreover, the appropriate training data size would be implied by comparing the training and blind test accuracy.

3.2.1. Extrapolation

Applying any extrapolation may cause low accuracy due to non-representativeness between training data and predicting data (Wang 2021).

We here use density contour of the training sample to define the potential extrapolation. A dozen of three-dimensional density contour surfaces are generated based on the distribution of training data. These surfaces are used as the boundary of the potential extrapolation. The magnitude combinations are (mag1, mag2, mag3), (mag2, mag3, mag4), ..., (mag12, mag1, mag2), and an example is shown in Fig. 4. The full name of each magnitude is shown in the figures. We present all the contour surfaces in Appendix A.

We then define the potential extrapolation with these 12 contour surfaces for the prediction. There are 3,496,867 (84.73%) objects of J-PLUS DR1 located inside these contours.

Table 3. Constitution of blind test set

Catalog	Interpolation	Extrapolation	Total
RAVE	64	6	70
KIC	3,168	195	3,363
2MRS	1,088	77	1,165
UVQS	52	41	93
Total	4,372	319	4,691

Notes. Every catalog are crossed with J-PLUS and make sure all 12 magnitudes are available. The extrapolation stands for the objects suffering potential extrapolating, and the other are interpolation.

3.2.2. Blind Test

We apply a blind test to reveal the classifier’s validation and its potential overfitting of the training data. The blind test data set (Table 3) is built by stars from Radial Velocity Experiment (RAVE) and Kepler Input Catalog (KIC), galaxies from 2 MASS (the Two Micron All Sky Survey) Redshift Survey (2MRS) and quasars from UV-bright Quasar Survey (UVQS). The accuracy distribution and the confusion matrix of the blind test are shown in Fig. 5 and 6.

RAVE is a stellar survey that focuses on obtaining stellar radial velocities (Steinmetz et al. 2020). It provides the spectroscopic parameters of stars with good accuracy. After cross matching with J-PLUS, we obtain only 70 stars, because RAVE is a southern survey. There are six stars suffering potential extrapolating. The number of stars is too small to validate our algorithm, so the KIC catalog is adopted to enlarged the blind test set. KIC catalog contains 3,363 stars in which 195 are extrapolations.

For galaxies in the blind test, we adopt the 2MRS catalog from Huchra et al. (2012). It is a red shift sky survey based on 2 MASS, including galaxies and QSOs with high red shift. There are 1,088 galaxies including 77 extrapolating ones.

We use UVQS catalog (Monroe et al. 2016) for QSO-blind testing, and obtain 93 objects after cross matching with J-PLUS. There are 41 objects fallen into the extrapolating region. UVQS contains UV bright QSOs, while VV13 is mainly in optical bands. This difference may cause bias between training and testing, and further result in different accuracies.

The blind test set is constructed by the four data sets. We select unique objects, and separate the testing data into the interpolating samples and those suffering potential extrapolation.

We also adopt some other parameters to describe the classifier: recall, precision, and F_1 -score. We first define True Positives (TP), False Positives (FP), and False Negatives (FN) to demonstrate these parameters. TP is the number that both the blind test labels and the predicted labels are positive. FP is the number that blind test labels are negative while the predicted labels are positive, FN is the number that blind test labels are positive, while the predicted labels are negative. Recall = $\frac{TP}{TP+FN}$, shows the fraction of right prediction for a label. Precision = $\frac{TP}{TP+FP}$, shows the fraction of right prediction. F_1 -score = $\frac{2}{\frac{1}{precision} + \frac{1}{recall}} = \frac{2TP}{2TP+FP+FN}$, shows the harmonic mean of the precision and the recall.

The total accuracy is 96.5% for the interpolating sample (Fig. 5 and 6), and the parameters are shown in Table 4. We present the accuracy distribution corresponding to the magnitudes as well (Fig. 9). The peak at 18m is probably due to the distribution overlap of stars, galaxies and QSOs. See more in Appendix B.

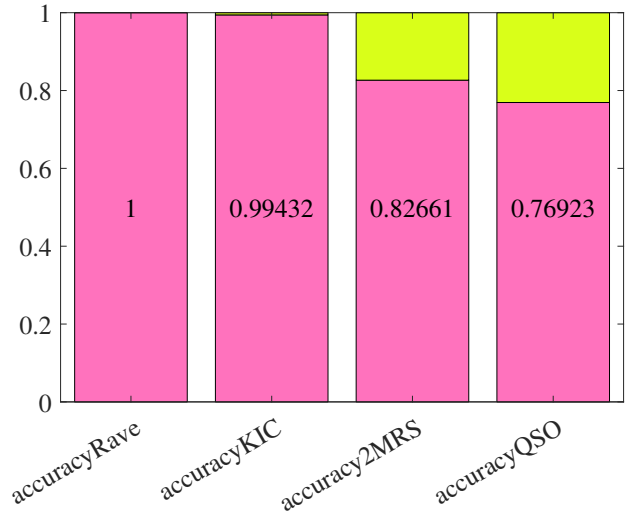


Fig. 5. The accuracy distribution for different interpolating data blind sets. The red bars show the correct objects, while the yellow bars show the incorrect ones. The numbers are the accuracies.

True Label	GALAXY	963		125		88.5%	11.5%
	QSO	5	40	7		76.9%	23.1%
	STAR	18		3214		99.4%	0.6%
		Predict Label					
		GALAXY	QSO	STAR			

Fig. 6. The confusion matrix for interpolating blind test, and the accuracy is 96.5%. The colors are same to Fig. 3

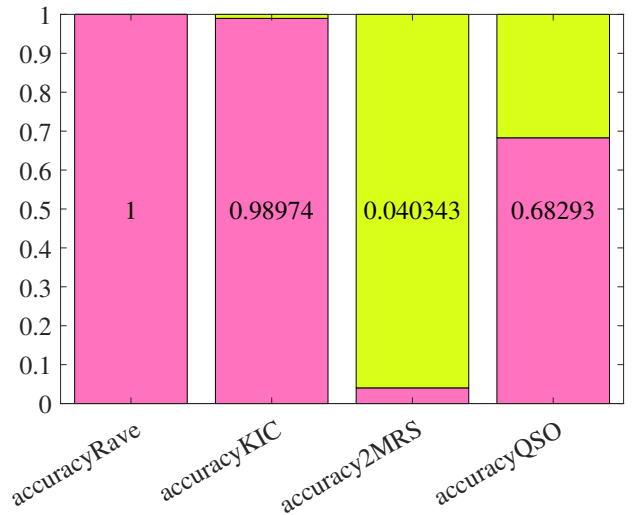


Fig. 7. The accuracy distribution for different extrapolating data blind sets. The colors are same to Fig. 5.

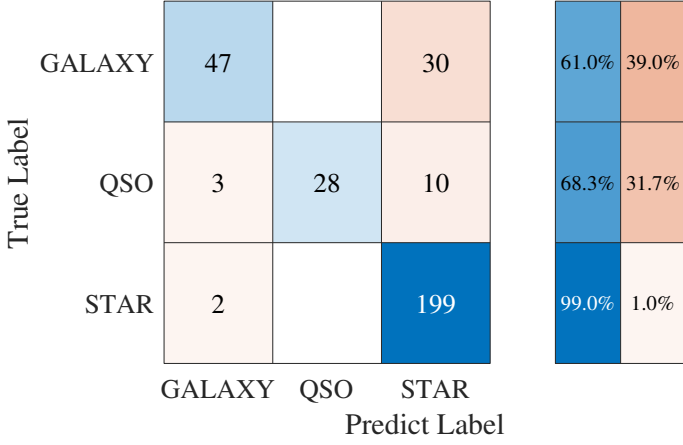


Fig. 8. The confusion matrix for the extrapolating blind test, and the accuracy is 85.9%.

Table 4. Parameters for interpolating blind test

Parameters	STAR	GALAXY	QSO
Recall	99.4%	88.5%	76.9%
Precision	96.1%	97.7%	1
F_1 -score	95.0%	92.9%	87.0%

Table 5. Parameters for extrapolating blind test

Parameters	STAR	GALAXY	QSO
Recall	99.0%	61.0%	68.3%
Precision	83.3%	90.4%	1
F_1 -score	90.5%	72.9%	81.2%

The blind test indicates a high reliability of the classifier. For the rest of the sample, the total accuracy is 85.9% (Fig. 7 and 8), much lower than the interpolating sample, and its parameters are shown in Table 5. This indicates that it is significant and effective to constrain extrapolation for prediction.

4. Results

The total number of objects in the J-PLUS data set is 13,265,168, and there are 4,126,928 objects with valid 12 magnitudes. We obtain a classifier using the 12-band magnitudes and their corresponding errors to classify objects into STAR, GALAXY and QSO. The classifier is constructed with SVM algorithm based on the data sets from J-PLUS, SDSS, LAMSOT, and VV13. We present a new classification catalog in Table 6. In order to avoid potential extrapolation, we have set up 12 contours and there are 3,496,867 objects located inside.

We have 2,493,424 stars, 613,686 galaxies, and 389,757 QSOs. The average probability is 95.63% for STAR, 86.62% for GALAXY, and 79.04% for QSO. We also present the color-color plot of these interpolating objects (Fig. 10, 11, and 12). In these plots, we choose $\text{mag6}-\text{mag8}$ and $\text{mag8}-\text{mag10}$ ($g-r$ and $r-i$) to show the spread of interpolating objects. We also provide the magnitude distributions of each class, see Appendix B.

The objects suffering potential extrapolation are shown in Table 7, including 223,924 stars, 239,616 galaxies and 166,521 QSOs, total 630,061 objects.

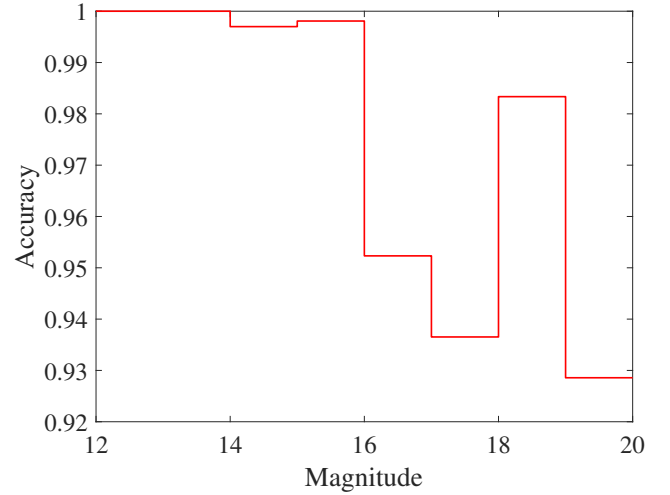


Fig. 9. The accuracy distribution correspond to mag5 (J0430). The x-axis shows the magnitudes, where the first stair presents the objects with magnitude brighter than 13, and the last present those fainter than 19. The magnitude bin is equal to 1.

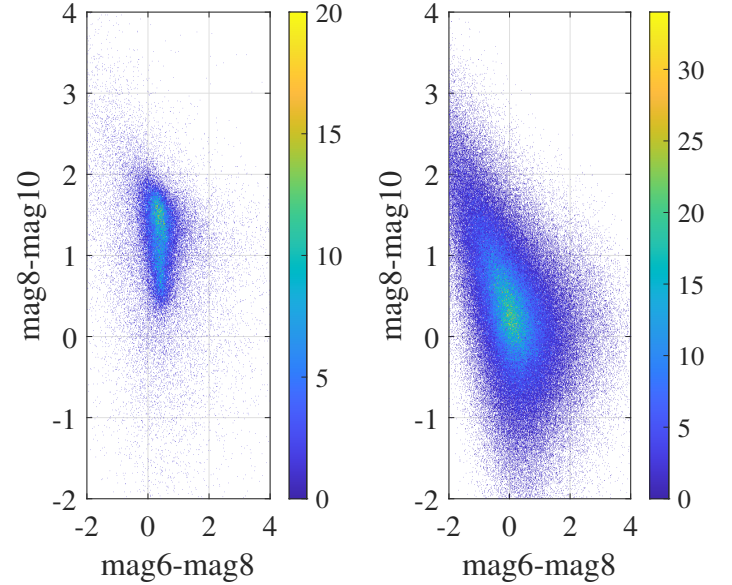


Fig. 10. The color-color diagram of GALAXYs. The left panel is the sample, and the right panel is the interpolation set. The color is the density of sample, with color bin of 0.01mag.

The classifier also presents the probabilities of three different classes, which enables us to select ambiguous objects. The ambiguous objects show characteristics that unlike any classes. When one's three-class probabilities are similar, it is selected as an ambiguous object. Table 8 shows different criteria and its corresponding object numbers. We present 155 objects with three probabilities lower than 0.34 in Table 9.

In order to find the abnormal objects from the ambiguous samples, we calculate the Mahalanobis distance (De Maesschalck et al. 2000; Mahalanobis 1936). We then check whether the objects are far to each label. The objects that have higher distance to one label than the distance of this label to the other labels are treated as abnormal objects. These objects are not only located outside the region of three classes, but also far from them. The criteria of Mahalanobis distance are: 18.4 from STAR to

Table 6. J-PLUS classification

ID	R.A.	Dec	class_star	PredictClass	Probability
26016-5	255.46	22.76	0.9990	STAR	92.96%
26016-15	255.30	22.76	0.9990	STAR	99.91%
26016-16	255.36	22.76	0.9990	STAR	99.20%
26016-22	255.27	22.76	0.9536	GALAXY	79.71%
26016-29	255.45	22.76	0.9814	GALAXY	76.31%
26016-33	255.39	22.76	0.9780	GALAXY	93.95%
26016-50	255.16	22.76	0.0460	STAR	64.35%
26016-55	255.66	22.76	1.0000	STAR	99.49%
26016-63	254.86	22.76	0.7656	QSO	86.82%
26016-64	254.75	22.76	0.9663	STAR	84.58%

Notes. This table contains the top 10 objects located inside the 12 contours. ID is the object identity from J-PLUS ^a. R.A. and Dec are the right ascension and declination of the objects. The column of class_star comes from J-PLUS catalog, denoting the probability of stars. The column of PredictClass presents our classification. The last column provides the probabilities of the predicted class. The sum of probabilities for the three classes is equal to 100%. In this work, we develop a SVM algorithm with one-vs-one strategy and gaussian kernel equal to 0.75. The table is uploaded with the paper.

^a <http://archive.cefca.es/catalogues/jplus-dr1/navigator.html>

Table 7. Objects suffering potential extrapolation

ID	RA	Dec	class_star	PredictClass	Probability
26016-2	255.64	22.75	0.9213	STAR	58.49%
26016-3	255.54	22.75	0.9345	STAR	60.68%
26016-9	255.39	22.76	0.4218	QSO	64.53%
26016-10	255.20	22.76	0.9497	STAR	64.68%
26016-11	255.40	22.76	0.9711	STAR	54.15%
26016-13	255.38	22.76	0.9604	STAR	96.74%
26016-14	255.22	22.76	0.9975	QSO	89.82%
26016-23	255.76	22.76	0.9379	QSO	95.45%
26016-34	255.61	22.76	0.6918	GALAXY	46.79%
26016-37	255.37	22.76	0.9785	STAR	95.16%

Notes. This table contains the top 10 objects located outside the 12 contours. The column label of this table is same to Table 6. The table is uploaded with the paper.

Table 8. Object number and criterion

Criterion	Object number
< 0.5	117,952
< 0.4	15,583
< 0.35	943
< 0.34	155

Notes. The criterion is the upper limit for the highest probability in three classes. The objects are picked up from both Table 6 and 7.

GALAXY, 23.3 from GALAXY to QSO, and 50.3 from QSO to STAR. Table 10 presents 26 abnormal objects.

In Fig. 13, we draw the difference between our results and the Class_Star in J-PLUS catalog. The figure indicates that there are differences between J-PLUS Class_Star and our result. The difference may cause by the different strategy of classifying the objects: binary classification for J-PLUS based on the point-source detection, and our triple classification based on machine learning. The QSOs are probably not distinguished from stars or galaxies with the point-source detection, and further result in the difference in Fig. 13. Therefore, the factor Class_Star may not be suitable enough for multi-classifications.

5. Discussion

5.1. Different ways to constrain extrapolation

We have construct three methods to constrain extrapolation, including magnitude cuts and two density-dependence methods.

The most straight forward way is defining intervals based on magnitude distributions of our training sample. We can determine whether an object belongs to the interpolation or extrapolation.

We employ kernel distribution (Bowman & Azzalini 1997) to fit the distributions of each dimension in the instance space. The kernel distribution is a probability measure. For each dimension, the objects in the middle part of the distribution are defined as interpolations. By cutting down 0.025 for each side of a magnitude distribution, the intervals are constructed, and the objects can be separated into interpolation or extrapolation. This method results in a accuracy of 95.4% for blind test. After the selection, there are 2,749,840 interpolating objects left, 65.79% of the J-PLUS catalog (Fig. 14 and 15). This method is precluded due to its low accuracy.

The ideal approach is to draw a 12-dimension density contour to select interpolating sample. The adopted method (Section 3.2.1) is an approximation of such ideal approach. The last method are four contours instead of 12 contours, which are

Table 9. First 10 objects of the ambiguous table

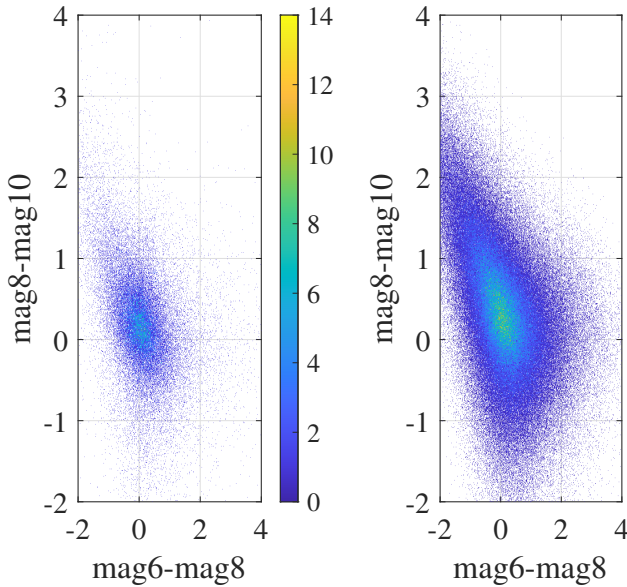
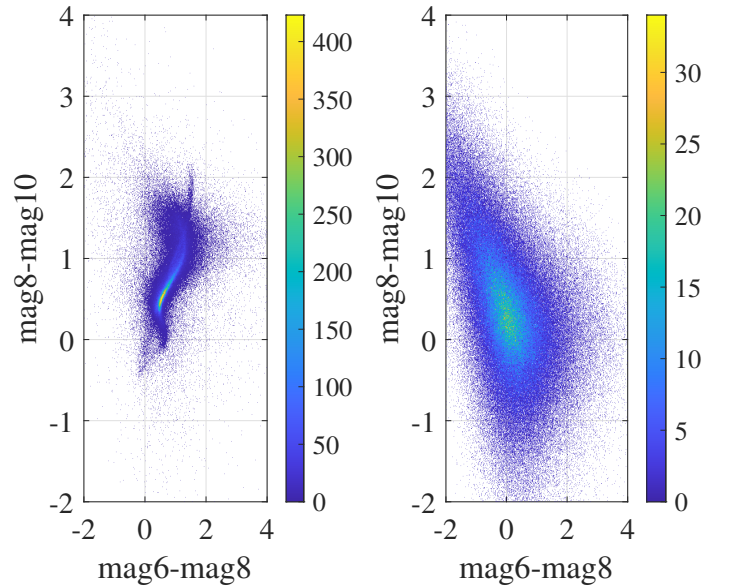
ID	RA	Dec	class_star	PredictClass	GALAXY	QSO	STAR
26016-20835	255.17	23.50	0.0008	GALAXY	33.50%	32.81%	33.68%
26016-32840	255.67	24.07	0.5004	STAR	33.38%	32.90%	33.70%
26015-6320	256.61	23.07	0.4304	STAR	32.54%	33.51%	33.94%
26010-33609	257.27	25.44	0.0078	GALAXY	33.71%	33.09%	33.19%
26012-8040	256.82	25.80	0.9121	GALAXY	33.95%	32.38%	33.65%
26012-24063	256.34	26.30	0.4980	GALAXY	33.25%	33.40%	33.33%
26028-3296	126.56	29.97	0.8632	STAR	32.39%	33.63%	33.97%
26037-3692	139.61	29.96	0.0011	GALAXY	33.45%	33.74%	32.80%
26038-17239	144.43	30.72	0.0027	QSO	33.22%	33.51%	33.25%
26036-8820	146.18	30.19	0.0050	GALAXY	33.45%	33.22%	32.82%

Notes. This table contains the top 10 ambiguous objects for criterion 0.34. The first five column labels of this table are the same as Table 6. The last three column mean the probability of corresponding label. The table is uploaded with the paper.

Table 10. First 10 objects of the abnormal table

ID	RA	Dec.	class_star	PredictClass	GALAXY	Gdis	QSO	Qdis	STAR	Sdis
26016-32840	255.67	24.08	0.5005	STAR	33.39%	45.85	32.90%	59.90	33.71%	214.59
26047-19730	121.32	31.91	0.0001	GALAXY	32.76%	78.09	33.94%	51.34	33.30%	204.47
26091-3622	128.45	34.13	0.4170	GALAXY	32.93%	201.06	33.70%	62.20	33.38%	391.73
33209-2012	137.46	39.61	0.1433	GALAXY	33.52%	55.05	32.89%	61.91	33.59%	224.79
26141-18524	169.58	40.47	0.0016	STAR	33.52%	73.44	32.63%	52.22	33.85%	185.80
26145-15610	284.79	39.72	0.2306	GALAXY	33.87%	133.31	32.82%	50.71	33.32%	278.23
33232-7122	126.08	41.30	0.1117	GALAXY	33.60%	98.28	33.32%	67.51	33.08%	251.50
26151-29824	273.32	41.61	0.0013	GALAXY	33.74%	229.37	32.77%	56.60	33.49%	255.62
26207-8959	137.27	52.63	0.0027	GALAXY	32.94%	66.90	33.75%	59.96	33.31%	312.61
26241-25002	243.42	54.58	0.5029	GALAXY	33.31%	129.51	33.41%	70.59	33.28%	278.00

Notes. This table contains the top 10 abnormal objects. The column labels of this table are the same as Table 9. The column Gdis, Qdis and Sdis mean the Mahalanobis distance to the group GALAXY, QSO and STAR. The table is uploaded with the paper.

**Fig. 11.** The color-color diagram of QSOs (similar to Fig. 10).**Fig. 12.** The color-color diagram of STARS (similar to Fig. 10).

(mag1, mag2, mag3), (mag4, mag5, mag6), (mag7, mag8, mag9) and (mag10, mag11, mag12). These rough contours result in an accuracy of 96.3%, and left 3,702,268 interpolating objects (Fig. 16 and 17). This method is also precluded due to its low accuracy.

5.2. Compare of different classifiers

Bai et al. (2018) used a random forest algorithm to gain a classifier with accuracy 99%. We also test random forest, but its accu-

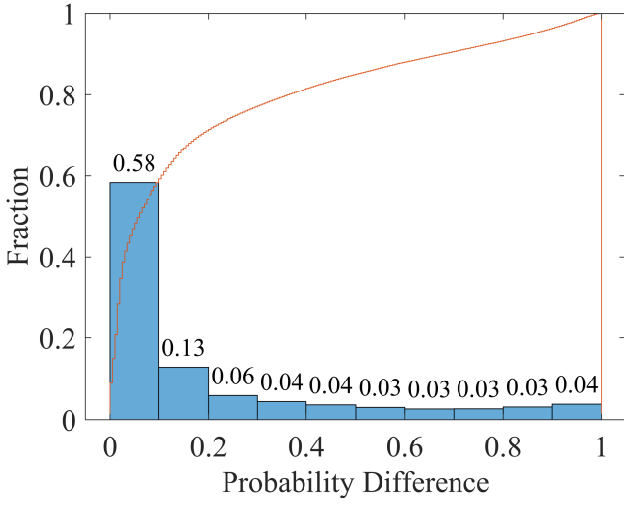


Fig. 13. The distributions of different probabilities between Class_Star and our stellar probabilities (blue bar). The red line shows the cumulative distribution function of the difference.

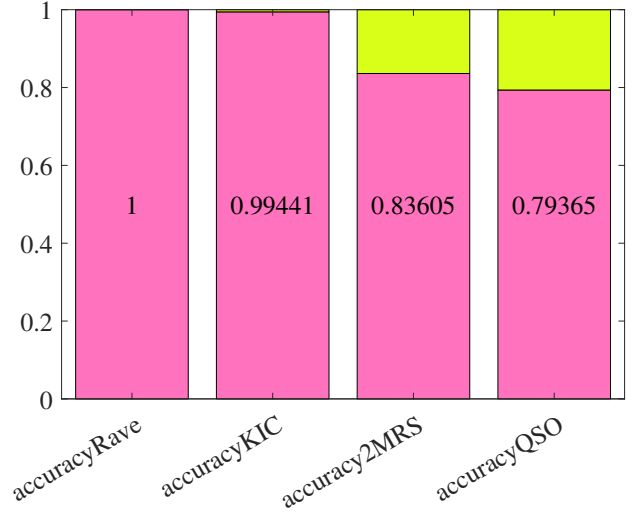


Fig. 16. The accuracy distribution for each blind test set under the rough contour method.

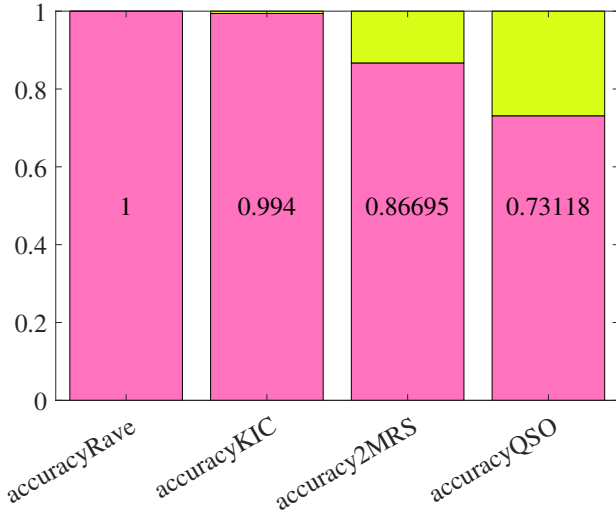


Fig. 14. The accuracy distribution for each blind test set under the kernel distribution method.

True Label	GALAXY	974		136	87.7%	12.3%
	QSO	5	50	8	79.4%	20.6%
	STAR	18		3266	99.5%	0.5%
		GALAXY QSO STAR			Predict Label	

Fig. 17. The confusion matrix of blind test by using the rough contour method to develop extrapolation, and the accuracy is 96.3%.

True Label	GALAXY	1010		151	87.0%	13.0%
	QSO	8	68	17	73.1%	26.9%
	STAR	18		2983	99.4%	0.6%
		GALAXY QSO STAR			Predict Label	

Fig. 15. The confusion matrix of blind test by using the kernel distribution method to develop the extrapolations, and the accuracy is 95.4%.

racy is lower than SVM. The different results of these two works probably due to the different sample sizes and wavebands.

The accuracy of blind test is similar to the training accuracy, implying that there is no obvious overfitting in our training process (Shalev-Shwartz & Ben-David 2014).

Sample size may also influence the training accuracy. In our method, the sample size is 468,685, while in Bai et al. (2018), the number is 2,973,855. Both SVM or random forest have finite Vapnik-Chervonenkis-dimension (VCdim; Shalev-Shwartz & Ben-David 2014). If a sample size goes to infinity, the training error and the validation error converge to the approximation error. This implies that there exist a limit accuracy of a classifier. In our work, the training error (97%) is similar to the validation error (96.5%). Therefore, if we enlarge the sample size, the accuracy may not increase significantly.

Bai et al. (2018) applied nine dimensional color space including infrared bands, while we use 12 optical magnitudes. More and broader bands involved in the training would lead to a higher total accuracy. The accuracy is slightly lower in our work. It probably due to the strong correlation in the 12 bands. We calculate a correlation matrix (Fig. 18) for these 12 bands from their photometric results.

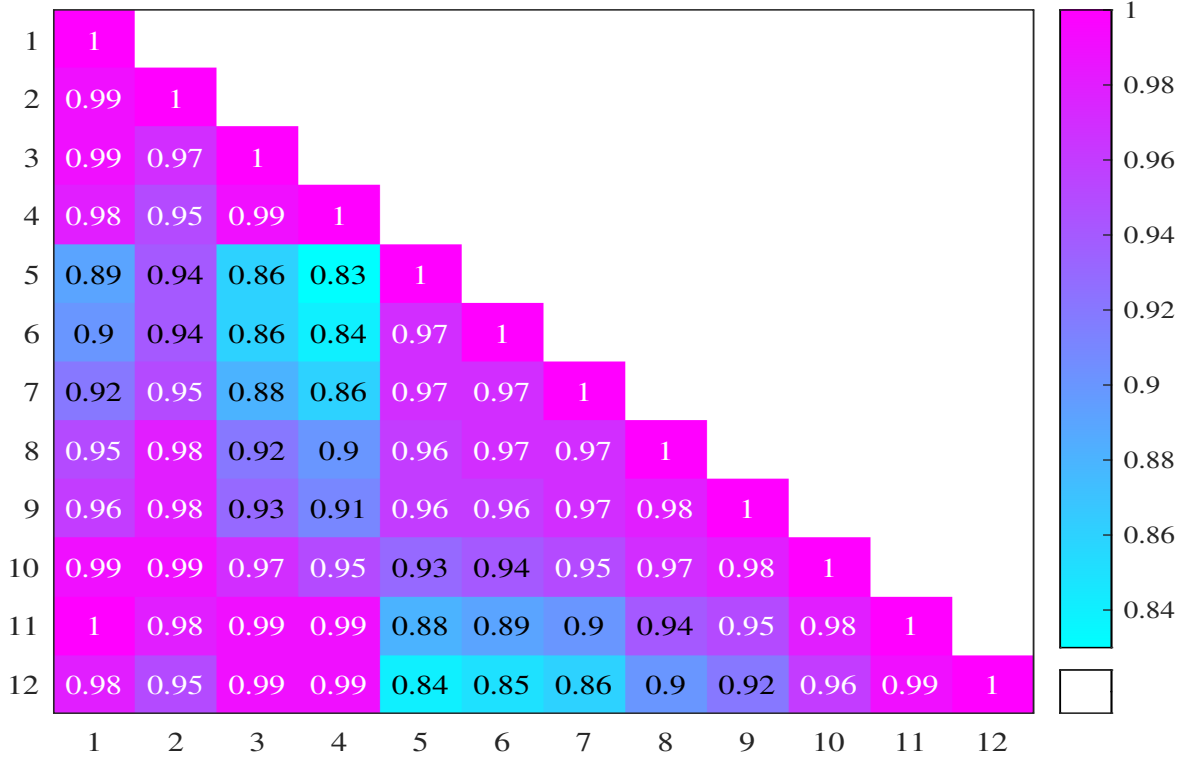


Fig. 18. The correlation matrix of the 12 bands. The numbers in the axes imply the bands, e.g. 1 for mag1. The 12 magnitudes are mag1 (u), mag2 (J0378), mag3 (J0395), mag4 (J0410), mag5 (J0430), mag6 (g), mag7 (J0515), mag8 (r), mag9 (J0660), mag10 (i), mag11 (J0861), mag12 (z).

Table 11. Constitution of different algorithms

Class	This work	Bai et al. (2018)	Ball et al. (2006)
Galaxy	15.94%	27.11%	75.77%
QSO(nsng)	9.79%	1.47%	11.16%
Star	74.27%	71.42%	13.07%

Notes. In Bai's paper, the second row is QSO, while in Ball's work, it's nsng.

The minimum of the correlation coefficient stands at (5, 4), mag4 (J0410) and mag5 (J0430) in Fig. 18. These high correlation values indicate that all of these wavebands are highly correlated. The correlation may be explained by not only the distance of the object that causes a similarity in all magnitudes, but also the overlapping of filter profiles. From the band plot in J-PLUS⁶, the filter profile of u , g , r , i , z have overlapping with other narrow bands, meaning that they are not strongly independent. The wavebands adopted in Bai et al. (2018) cover a larger range, and the correlations are probably weaker.

The constitute of data set may also influence the accuracy of a classifier, but its significance is worthy to discuss. In Ball et al. (2006), a tree algorithm is developed to output the probability of star, galaxy and nsng (neither star nor galaxy object). In Bai's and Ball's training sample, there is a significant bias in the sample set. The sample construction of our SVM classifier and the two mentioned classifier is shown in Table 11.

⁶ The plot can be find both in http://www.j-plus.es/ancillarydata/dr1_lya_emitting_candidates, and the paper of J-PLUS (Cenarro et al. 2019)

Bai et al. (2018) and Ball et al. (2006) concluded that the biased sample can also present a well accuracy, while they also resulted in high accuracy in cross validation.

5.3. Future work

The advantages of J-PLUS are 12 optical filters and large amount of data. The on-going J-PAS has an "unprecedented system of 56 optical narrow band filters", making it one of the most promising surveys in the world. The way we work on J-PLUS is the way tomorrow on J-PAS. The more bands applied, the more precise a classifier could achieve.

Baqui, P. O. et al. (2021), developed different classifiers to label the mini-JPAS (Bonoli et al. 2021), including RF and Extremely Randomized Trees (ERT). MiniJ-PAS is a precedent project to test J-PAS. Their work has gained a well performance with Area Under the Curve (AUC) greater than 0.95 in different classifiers. AUC is equal to the positive probability.

SVM is inferior when the instance space has too many dimensions, or when the data set is too large for calculation. More works are required to test the time cost of SVM, when we apply larger data with more features. However, the no-free-lunch theorem concludes that there is no perfect learning algorithm that can classify everything. SVM is a good algorithm, but its performance in J-PAS is still needed to be tested.

Acknowledgements. This work was supported by the National Natural Science Foundation of China (NSFC) through grants NSFC-11988101/11973054/11933004 and the National Programs on Key Research and Development Project (grant No.2019YFA0405504 and 2019YFA0405000). Strategic Priority Program of the Chinese Academy of Sciences under grant number XDB41000000. H. B. Yuan, acknowledge funding from National Natural Science Foundation of China (NSFC) through grants NSFC-12173007. ELM acknowledges support from the Agencia Estatal de Investigación del Ministerio de Ciencia e Innovación (AEI-MCINN) under grant PID2019-109522GB-C53.

Based on observations made with the JAST80 telescope at the Observatorio Astrofísico de Javalambre (OAJ), in Teruel, owned, managed, and operated by the Centro de Estudios de Física del Cosmos de Aragón (CEFCA). We acknowledge the OAJ Data Processing and Archiving Unit (UPAD) for reducing the OAJ data used in this work. Funding for the J-PLUS Project has been provided by the Governments of Spain and Aragón through the Fondo de Inversiones de Teruel; the Aragón Government through the Research Groups E96, E103, and E16_17R; the Spanish Ministry of Science, Innovation and Universities (MCIU/AEI/FEDER, UE) with grants PGC2018-097585-B-C21 and PGC2018-097585-B-C22; the Spanish Ministry of Economy and Competitiveness (MINECO) under AYA2015-66211-C2-1-P, AYA2015-66211-C2-2, AYA2012-30789, and ICTS-2009-14; and European FEDER funding (FCDD10-4E-867, FCDD13-4E-2685). The Brazilian agencies FINEP, FAPESP, and the National Observatory of Brazil have also contributed to this project. Guoshoujing Telescope (the Large Sky Area Multi-Object Fiber Spectroscopic Telescope LAMOST) is a National Major Scientific Project built by the Chinese Academy of Sciences. Funding for the project has been provided by the National Development and Reform Commission. LAMOST is operated and managed by the National Astronomical Observatories, Chinese Academy of Sciences. Funding for the Sloan Digital Sky Survey IV has been provided by the Alfred P. Sloan Foundation, the U.S. Department of Energy Office of Science, and the Participating Institutions. SDSS-IV acknowledges support and resources from the Center for High-Performance Computing at the University of Utah. The SDSS website is <http://www.sdss.org/>. SDSS-IV is managed by the Astrophysical Research Consortium for the Participating Institutions of the SDSS Collaboration including the Brazilian Participation Group, the Carnegie Institution for Science, Carnegie Mellon University, the Chilean Participation Group, the French Participation Group, Harvard-Smithsonian Center for Astrophysics, Instituto de Astrofísica de Canarias, The Johns Hopkins University, Kavli Institute for the Physics and Mathematics of the Universe (IPMU)/University of Tokyo, Lawrence Berkeley National Laboratory, Leibniz Institut für Astrophysik Potsdam (AIP), Max-Planck-Institut für Astronomie (MPIA Heidelberg), Max-Planck-Institut für Astrophysik (MPA Garching), Max-Planck-Institut für Extraterrestrische Physik (MPE), National Astronomical Observatories of China, New Mexico State University, New York University, University of Notre Dame, Observatório Nacional/MCTI, The Ohio State University, Pennsylvania State University, Shanghai Astronomical Observatory, United Kingdom Participation Group, Universidad Nacional Autónoma de México, University of Arizona, University of Colorado Boulder, University of Oxford, University of Portsmouth, University of Utah, University of Virginia, University of Washington, University of Wisconsin, Vanderbilt University, and Yale University. This work is supported by the CSST project on "stellar activity and late evolutionary stage".

References

- Ahumada, R., Allende Prieto, C., Almeida, A., et al. 2020, *ApJS*, 249, 3
- Bai, Y., Liu, J., Wang, S., & Yang, F. 2018, *The Astronomical Journal*, 157, 9
- Ball, N. M., Brunner, R. J., Myers, A. D., & Tchong, D. 2006, *The Astrophysical Journal*, 650, 497–509
- Baqui, P. O., Marra, V., Casarini, L., et al. 2021, *A&A*, 645, A87
- Benítez, N., Dupke, R., Moles, M., et al. 2014, [ArXiv:1403.5237] [arXiv:1403.5237]
- Bertin, E. & Arnouts, S. 1996, *A&AS*, 117, 393
- Bonoli, S., Marín-Franch, A., Varela, J., et al. 2021, *A&A*, 653, A31
- Boser, B. E., Guyon, I. M., & Vapnik, V. N. 1992, in *Proceedings of the Fifth Annual Workshop on Computational Learning Theory, COLT '92* (New York, NY, USA: Association for Computing Machinery), 144–152
- Bowman, A. W. & Azzalini, A. 1997, *Applied smoothing techniques for data analysis: the kernel approach with S-Plus illustrations*, Vol. 18 (OUP Oxford)
- Breiman, L. 2001, *Statist. Sci.*, 16, 199
- Cenarro, A. J., Moles, M., Cristóbal-Hornillos, D., et al. 2019, *Astronomy & Astrophysics*, 622, A176
- Cenarro, A. J., Moles, M., Marín-Franch, A., et al. 2014, in *Proc. SPIE*, Vol. 9149, *Observatory Operations: Strategies, Processes, and Systems V*, 91491I
- Cortes, C. & Vapnik, V. 1995, *Machine Learning*, 20, 273
- Cover, T. & Hart, P. 1967, *IEEE Trans. Inf. Theory*, 13, 21
- Cristianini, N. & Shawe-Taylor, J. 2000, *An Introduction to Support Vector Machines and Other Kernel-based Learning Methods* (Cambridge University Press)
- Cui, X.-Q., Zhao, Y.-H., Chu, Y.-Q., et al. 2012, *Research in Astronomy and Astrophysics*, 12, 1197
- De Maesschalck, R., Jouan-Rimbaud, D., & Massart, D. 2000, *Chemometrics and Intelligent Laboratory Systems*, 50, 1
- Deng, L.-C., Newberg, H. J., Liu, C., et al. 2012, *Research in Astronomy and Astrophysics*, 12, 735
- FISHER, R. A. 1936, *Annals of Eugenics*, 7, 179
- Freund, Y. & Schapire, R. E. 1995, *A Decision-Theoretic Generalization of on-Line Learning and an Application to Boosting*
- guan Wang, S., qiang Su, D., quan Chu, Y., Cui, X., & nan Wang, Y. 1996, *Appl. Opt.*, 35, 5155
- Huchra, J. P., Macri, L. M., Masters, K. L., et al. 2012, *The Astrophysical Journal Supplement Series*, 199, 26
- Jiménez-Teja, Y., Dupke, R. A., Lopes de Oliveira, R., et al. 2019, *Astronomy & Astrophysics*, 622, A183
- López-Sanjuan, C., Vázquez Ramió, H., Varela, J., et al. 2019, *A&A*, 622, A177
- Luo, A.-L., Zhang, H.-T., Zhao, Y.-H., et al. 2012, *Research in Astronomy and Astrophysics*, 12, 1243
- Mahalanobis, P. C. 1936, *Proceedings of the National Institute of Sciences (Calcutta)*, 2, 49
- Marín-Franch, A., Taylor, K., Cenarro, J., Cristóbal-Hornillos, D., & Moles, M. 2015, in *IAU General Assembly*, Vol. 29, 2257381
- Monroe, T. R., Prochaska, J. X., Tejos, N., et al. 2016, *The Astronomical Journal*, 152, 25
- Nogueira-Cavalcante, J. P., Dupke, R., Coelho, P., et al. 2019, *Astronomy & Astrophysics*, 630, A88
- Quinlan, J. R. 1986, *Machine Learning*, 1, 81
- Shalev-Shwartz, S. & Ben-David, S. 2014, *Understanding Machine Learning: From Theory to Algorithms* (Cambridge University Press)
- Steinmetz, M., Matijević, G., Enke, H., et al. 2020, *The Astronomical Journal*, 160, 82
- Stone, C. J. 1977, *The Annals of Statistics*, 5, 595
- Su, D.-Q. & Cui, X.-Q. 2004, *Chinese journal of Astronomy and Astrophysics*, 4, 1
- Véron-Cetty, M. P. & Véron, P. 2010, *A&A*, 518, A10
- Wang, S. 2021, Private communication
- Whitten, D. D., Placco, V. M., Beers, T. C., et al. 2019, *Astronomy & Astrophysics*, 622, A182
- Yuan, H. 2021, In preparation and private communication
- Yuan, H., Liu, X., Xiang, M., et al. 2015, *The Astrophysical Journal*, 799, 133
- Zasowski, G., Johnson, J. A., Frinchaboy, P. M., et al. 2013, *The Astronomical Journal*, 146, 81
- Zhao, G., Zhao, Y.-H., Chu, Y.-Q., Jing, Y.-P., & Deng, L.-C. 2012, *Research in Astronomy and Astrophysics*, 12, 723

Appendix A: Contours

We present all 12 three-dimensional contours of the predictions.

Appendix B: Magnitude distributions

We present the magnitude distributions for each class, magnitude and for both sample and interpolations. The red line indicate STAR, the green for GALAXY and blue for QSO. The x-axis shows the magnitude, and the y-axis shows the probability.

Appendix C: Sample of our training

We present the training sample here, and subclass of STARs are included.

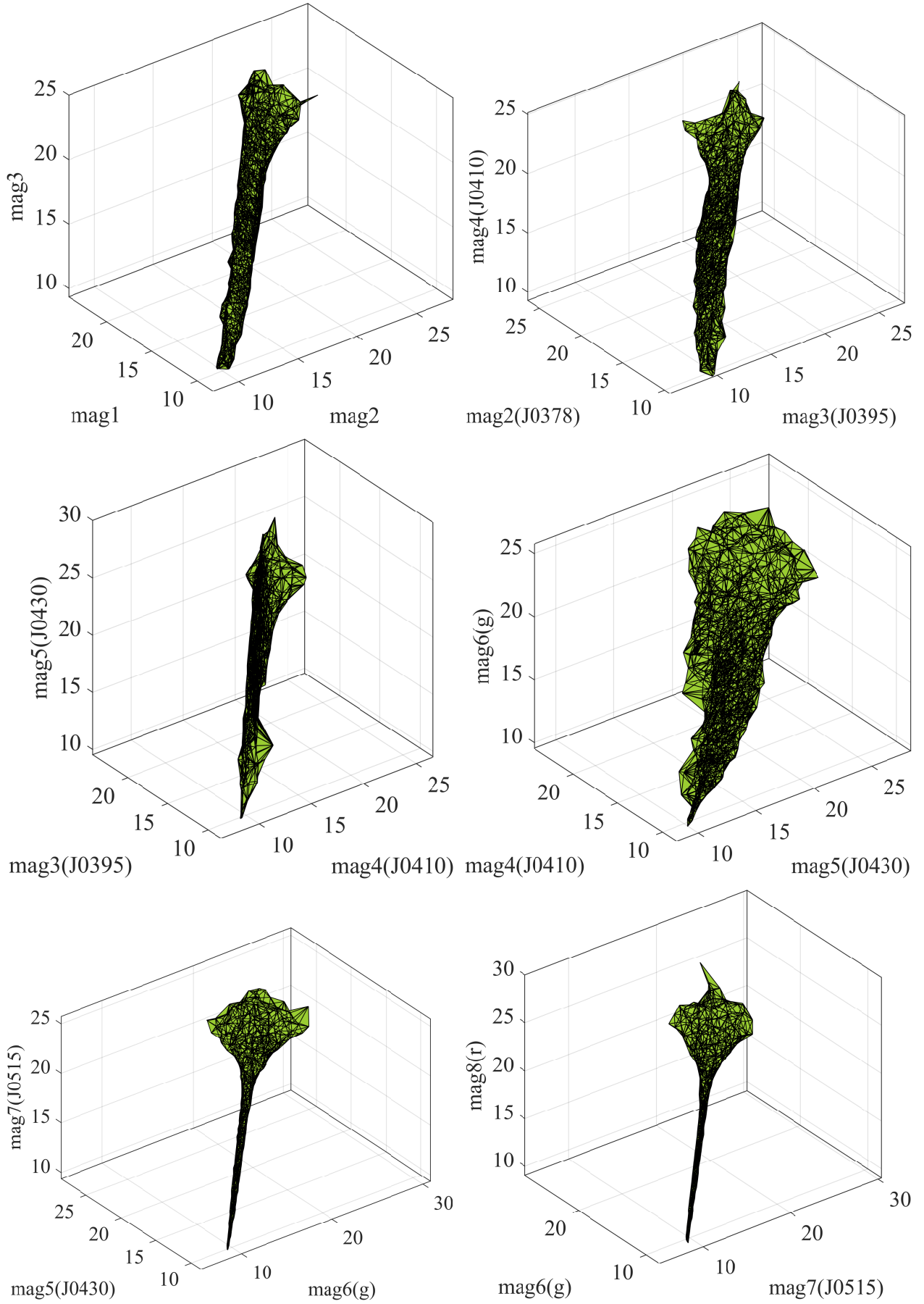


Fig. A.1. The first six contours for extrapolation controlling.

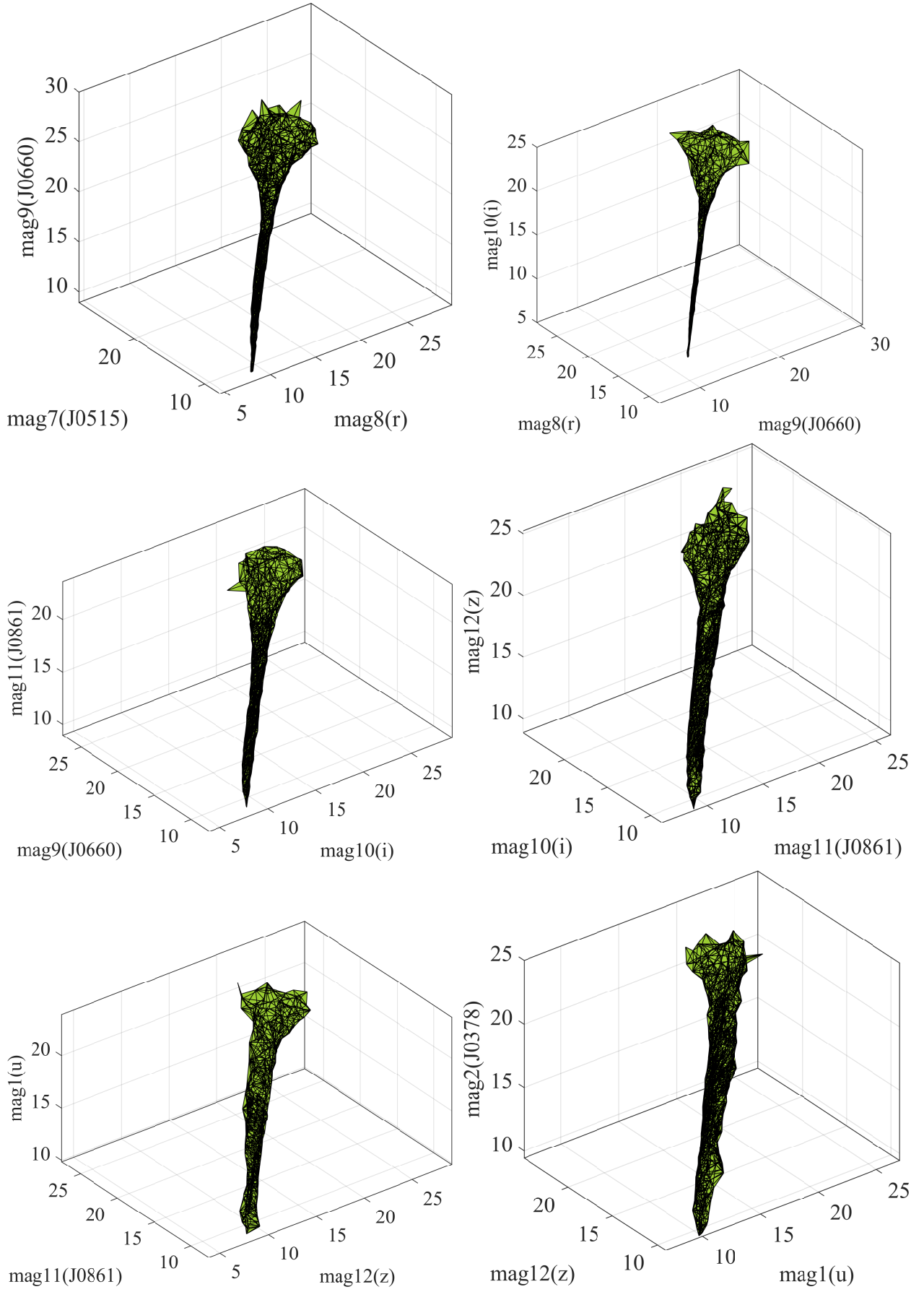


Fig. A.2. The last six contours for extrapolation controlling.

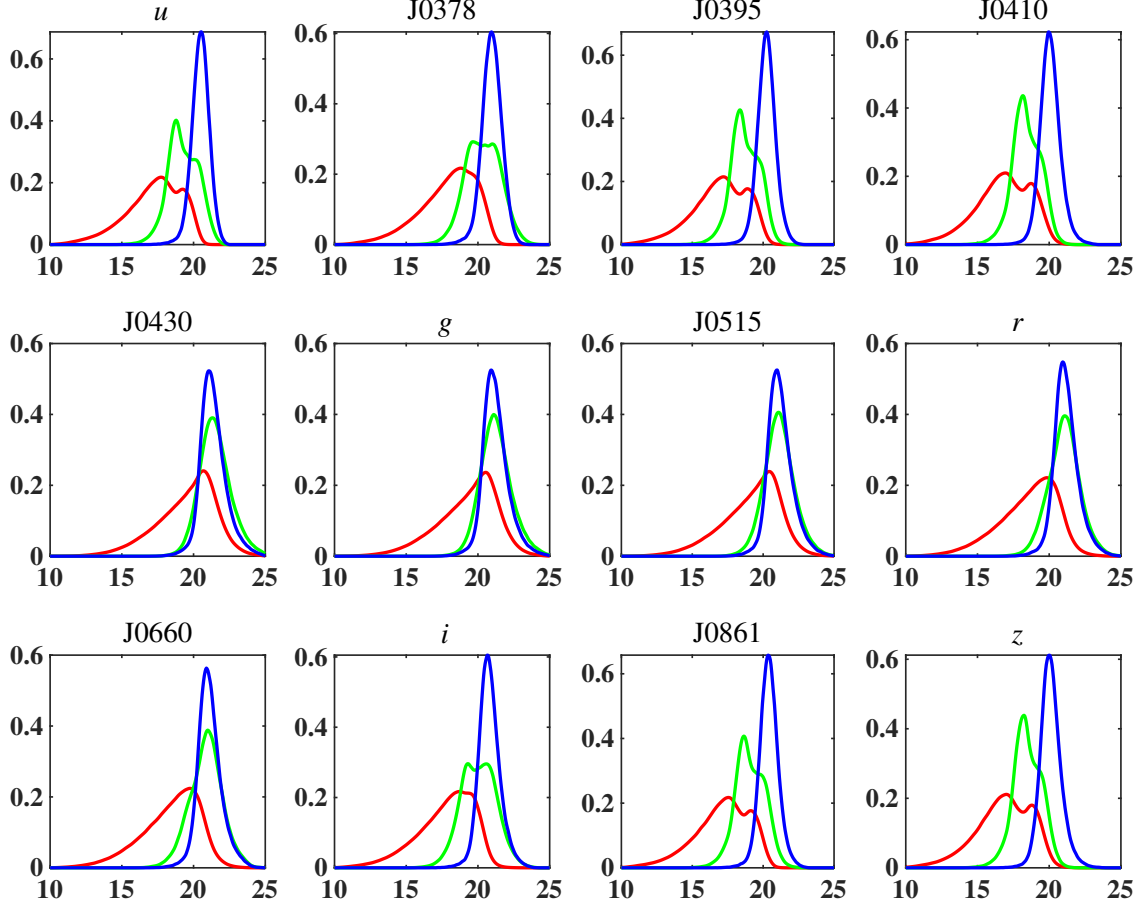


Fig. B.1. The magnitude distributions for the interpolation objects. The STARS are red. The GALAXYs are green, and the QSOs are blue.

Table C.1. Training sample

ID	R.A.	Dec.	class	subclass	catalog
25998-850	117.07	39.50	STAR	M0	LAMOST
25998-912	116.27	39.48	STAR	M0	LAMOST
25998-913	117.39	39.49	STAR	K7	LAMOST
25998-932	116.06	39.50	STAR	M2	LAMOST
25998-942	116.99	39.50	GALAXY	Non	LAMOST
25998-969	116.48	39.51	QSO	Non	LAMOST
25998-971	117.53	39.50	STAR	Non	LAMOST
25998-972	117.63	39.50	STAR	K7	LAMOST
25998-977	116.49	39.49	STAR	G7	LAMOST
25998-1015	117.34	39.50	STAR	K5	LAMOST
25998-1033	116.30	39.51	STAR	Non	LAMOST

Notes. The first four columns are the same as Table 6. The 'subclass' is labeled from LAMOST catalog, indicating the subclass of stars. The 'Non' means missing subclass or not a star. 'Catalog' shows the origin catalog.

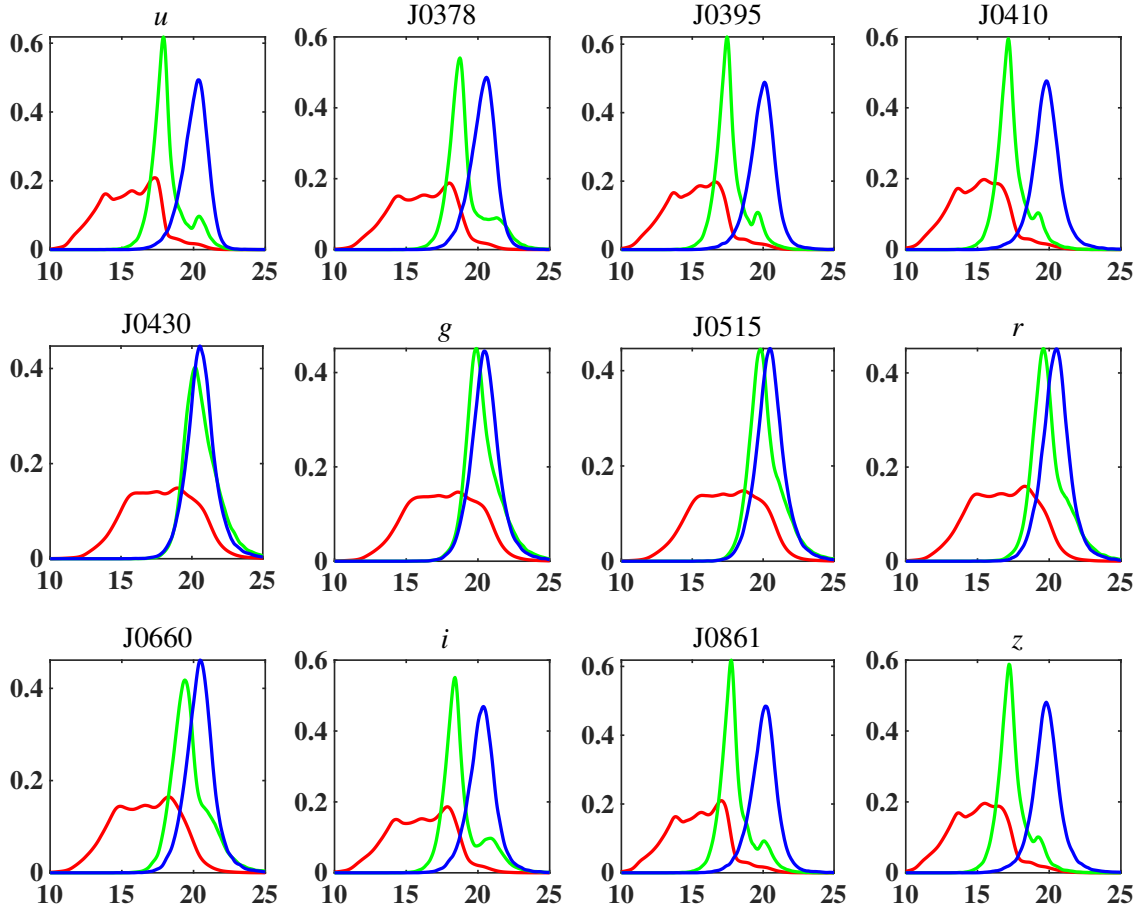


Fig. B.2. The magnitude distribution for sample objects. The line colors are the same as the interpolations.